applied sciences

MDPI

Article

A Variable-Order Dynamic Constitutive Model for Clay Based on the Fractional Calculus

Bo-Lang Zhang, Kai-Sheng Chen *, Xing Hu and Kun Zhang

School of Civil Engineering, Guizhou University, Guiyang 550025, China; bolangzhang123@163.com (B.-L.Z.); xhu1@gzu.edu.cn (X.H.); m18148410075@163.com (K.Z.)
* Correspondence: kschen@gzu.edu.cn

Abstract: To accurately describe the deformation characteristics of clay under long-term cyclic load, based on fractional calculus theory, elastoplastic theory and the basic element model, a variable-order fractional dynamic model designed to predict accumulative strain of clay was exhibited. Firstly, the cyclic load was separated into static and alternating load in accordance with cyclic load characteristics, and the strain of clay under static and alternating load was analyzed. Then, on the basis of the variable-order Abel dashpot model, rheological theory and elastoplastic theory, the expressions of the rheological constitutive model and strain response were both obtained. Finally, in combination with the undrained dynamic triaxial testing of Zhan Jiang clay and Tian Jin soft clay, a series of analyses was carried out on the effectiveness and parameter sensitivity of the model when subjected to long-term cyclic loading. By comparing the dynamic constitutive model with pre-existing models, the superiority of the dynamic constitutive model is revealed. The results show that the dynamic constitutive model can characterize properly the deformation characteristics of clay under the action of long-term cyclic loading, especially in its accelerating stage. The parameter sensitivity of the model exhibits a growing trend with the increment of loading duration.

Keywords: dynamic constitutive model; variable-order Abel dashpot; parameter sensitivity; element model; deformation characteristics

Citation: Zhang, B.-L.; Chen, K.-S.; Hu, X.; Zhang, K. A Variable-Order Dynamic Constitutive Model for Clay Based on the Fractional Calculus. *Appl. Sci.* **2022**, *12*, 6416. https://doi.org/10.3390/app12136416

Academic Editors: José M. Vega, Hamed Farokhi, Roman Starosta, Jan Awrejcewicz, José A. Tenreiro Machado, Hari Mohan Srivastava and Ying-Cheng Lai

Received: 15 May 2022
Accepted: 22 June 2022
Published: 24 June 2022

1. Introduction

Clay, such as soft clay or silt. is an elastic-viscoplastic material with high water content and compressibility [1–3]. Due to its low bearing capacity, a large secondary settlement in infrastructure constructions (expressways, metro tunnels, airstrips, etc.) built on a clay foundation occurs readily under the action of cyclic loading, which directly affects operational usage and can generate considerable reconstruction expense [4,5]. Consequently, it is essential to conduct research about accumulative strain of clay subjected to cyclic loading.

Accumulative strain of clay subjected to cyclic loading will increase along with loading duration, and various constitutive models designed to predict the accumulative strain upon soil have been proposed by many scholars. To date, these models can be roughly separated into theoretical models and empirical models, according to their method of data acquisition; the former are generally more complex compared to the latter, and a great diversity of models have been obtained due to the various theories adopted by scholars. Based on elastoplastic theory, many dynamic constitutive models capable of predicting accumulative strain of soil have been proposed [6–9]. With the introduction of numerical simulation approaches, several authors have developed constitutive models to capture the effects of cyclic loading on traffic settlement [10–12]. Furthermore, based on general thermodynamic principles and Newton's laws of motion, Deng and other authors [13]

presented a constitutive model to explore the dynamic response of soft clay under dynamic loads. Although these theoretical models have good ability in predicting the accumulative deformation of soil, the complexity of their equations has inhibited their popularity in engineering contexts, Empirical models are obtained by fitting mass data to curves of accumulative plastic strain-times of curve, and an empirical model was first exhibited by Monismith [14]. Subsequently, taking into consideration the differences in the mechanical properties of various soils, scholars have proposed different dynamic constitutive models for fine-grained soils [15], saturated soft clay [16], peaty soil [17], silt sand [18], frozen clay [19], compacted loess [20] etc. In addition, scholars have carried out extensive experiments to explore the effects of intermittent loading, loading characteristics, variable confining pressures, principal stress rotation and other factors affecting the mechanical properties and deformation characteristics of soil [21–24]. Because of their simplicity and desirable ability to predict material behavior, empirical model formulas are now widely applied in practical engineering.

Nevertheless, the parameters in empirical models have the weakness of being susceptible to experimental circumstances which greatly limits the ability of these models to predict accumulative deformation of soil. Element models, as one of the traditional rheological constitutive models, are utilized by engineers and researchers for describing the deformation characteristics of geotechnical materials because of their simple concepts and explicit physical meanings. For instance, Kabwe et al. [25] derived a fractional-order derivative viscoelastic–viscoplastic constitutive model capable of estimating delayed deformations characterized by squeezing. Based on the Nishihara model, Song et al. [26] constructed a fatigue deformation model by introducing a nonlinear function to reflect the entire process of the irreversible accumulation deformation of limestone under osmotic pressure and cyclic disturbance coupling. Zhu et al. [27] proposed a new nonlinear creep constitutive model by introducing a damage variable into the viscoplastic element to accurately describe the whole creep process for frozen sand with different dry densities and grain size distributions under different shear stress levels and temperatures. Analogously, to capture the deformation behavior of various geotechnical materials under different mechanical states, authors [28–33] constructed a series of significant constitutive models suitable for describing the accumulative deformation of geotechnical materials under static loading. However, element models used to depict the deformation characteristics of geotechnical materials under dynamic loads are comparatively few, though there are some research results in the literature. By connecting constructed fractional-order viscoplastic bodies, Pu et al. [34] constructed a novel constitutive equation using Burgers' model to portray the deformation of rock under cyclic loading. Therefore, as well as seeking better methods to describe the deformation characteristics of soil under the action of dynamic loading, it is essential to conduct further research into element models.

This study separated the cyclic load into static and alternating loads. Using fractional calculus and elastoplastic theory, we obtained the amplitude of creep under static load, and the value of strain response under alternating load, respectively. Then, the results of dynamic triaxial test were used to study the constitutive model's effectiveness under dynamic loads, and the sensitivity of parameters. Through a comparison between different constitutive models, the advantage of our constitutive model was then revealed.

2. Theory of Clay Deformation under Cyclic Loading

2.1. Analysis of Cyclic Stress

Based on domestic and international research experience, it is assumed that the wave of cyclic load applied to the clay surface is a half sine wave, so cyclic stress is given as follows Figure 1.

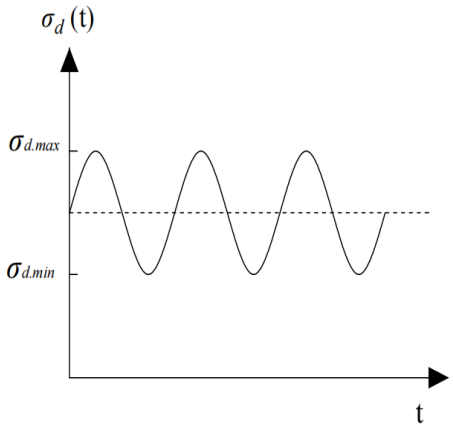

Figure 1. Diagrammatic sketch of cyclic stress.

$$\sigma_d(t) = \frac{\sigma_{\mathrm{d.max}} + \sigma_{\mathrm{d.min}}}{2} + \frac{(\sigma_{\mathrm{d.max}} - \sigma_{\mathrm{d.min}})}{2} sin(\omega t) \quad (1)$$

where ω is the angular frequency, $\sigma_d(t)$, and $\sigma_{\mathrm{d.max}}$ and $\sigma_{\mathrm{d.min}}$ are the maximum and the minimum levels of cyclic stress, respectively.

Obviously, cyclic stress shown in Figure 1 can be separated into static load $\sigma_s(t)$ and alternating load $\sigma_a(t)$. Figure 2a,b show static stress and alternating stress, respectively.

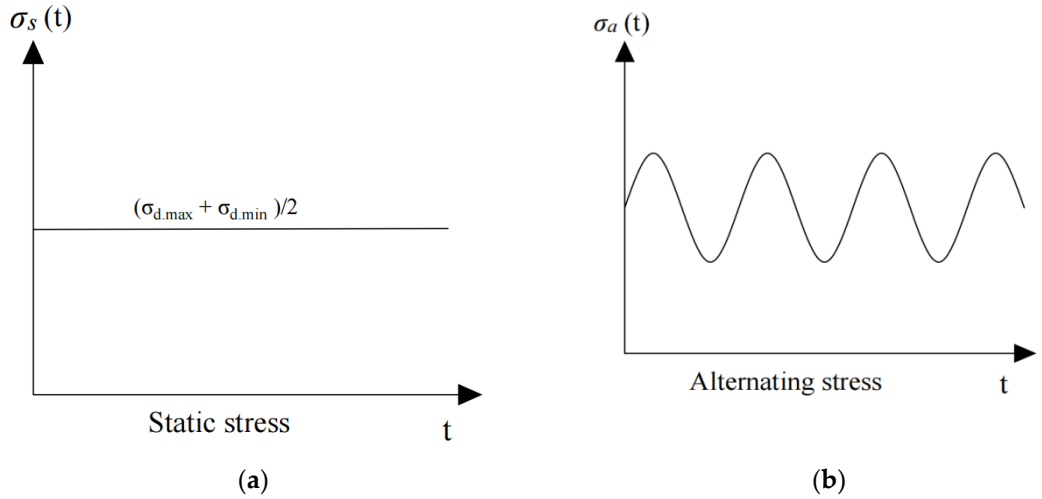

(**a**) (**b**)

Figure 2. (**a**) Diagrammatic sketch of static stress; (**b**) Diagrammatic sketch of alternating stress.

The static stress $\sigma_s(t)$ and the alternating stress $\sigma_a(t)$ in accordance with the above analysis can be expressed as

$$\sigma_s(t) = \frac{\sigma_{\mathrm{d.max}} + \sigma_{\mathrm{d.min}}}{2} \quad (2)$$

$$\sigma_a(t) = \frac{(\sigma_{\mathrm{d.max}} - \sigma_{\mathrm{d.min}})}{2} sin(\omega t) \quad (3)$$

2.2. Deformation Characteristics of Clay under Different Loads

2.2.1. Deformation Characteristics of Clay under Long-Term Static Load

Due to the nonlinear creep property of clay, the total strain $\varepsilon_s(t)$ under constant static load consists of both instantaneous and creep strain [35], so that.

$$\varepsilon_s(t) = \varepsilon_e + \varepsilon_c(t) \tag{4}$$

where ε_e is instantaneous strain, and $\varepsilon_c(t)$ is creep strain, which contains the viscoelastic strains $\varepsilon_{ve.1}$ and $\varepsilon_{ve.2}$ in the initial creep and steady creep stages of the loading process, respectively, and the viscoplastic strain ε_{vp} in the accelerating creep stage. Figure 3 shows the representative creep strain-time curve for clay under long-term static load.

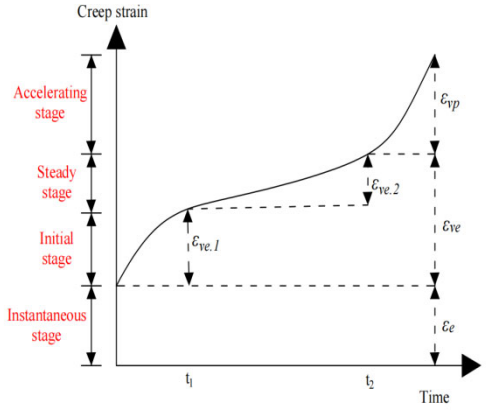

Figure 3. Representative creep strain-time curve of clay.

During initial creep, we calculate

$$\varepsilon_s(t) = \varepsilon_e + \varepsilon_{ve.1}(t) \qquad (0 < t \le t_1) \tag{5}$$

During steady creep, we calculate

$$\varepsilon_s(t) = \varepsilon_e + \varepsilon_{ve.1} + \varepsilon_{ve.2}(t) \qquad (t_1 < t \le t_2) \tag{6}$$

During accelerating creep, we calculate

$$\varepsilon_s(t) = \varepsilon_e + \varepsilon_{ve.1} + \varepsilon_{ve.2} + \varepsilon_{vp}(t) \qquad (t_2 < t) \tag{7}$$

In all, the total representative creep process of clay of consists four parts: instantaneous stage, initial stage, steady stage, and accelerating stage. It is worth noting that the creep properties of clay are associated with stress levels, matric suction, consolidation and other factors [36–39].

2.2.2. Deformation Characteristics of Clay under Alternating Load

The accumulative plastic strain-time curves of geotechnical materials under long-term alternating load can be categorized into three types [40]: (1) steady curve; (2) critical curve; (3) failure curve, as shown in Figure 4a. The dynamic stress that makes an accumulative strain-time curve evolve into a critical curve is called critical dynamic stress σ_{cr}, and accumulative strain-time curves evolve into steady or failure curves, depending on whether the dynamic stress is lower or higher than σ_{cr}. The rate of a steady curve is faster in the initial stage before settling into a constant level, the rate of a critical curve is characterized by fluctuation, while the rate of accumulative plastic strain increases with loading duration for the failure curve. However, it is laborious to obtain ideal experimental data as depicted in Figure 4a. More typically, accumulative plastic strain-time data such as we obtained resembles Figure 4b, where failure and steady curves are primarily distributed in the upper left and lower right regions of the figure, while critical curves are distributed in the grey region between them. Experimental tests can only obtain a range of critical dynamic stress, so it is hard to obtain the precise value of critical dynamic stress by laboratory testing [41]. For this reason, the critical dynamic stress σ_{cr} is taken to be the median of the range in this paper.

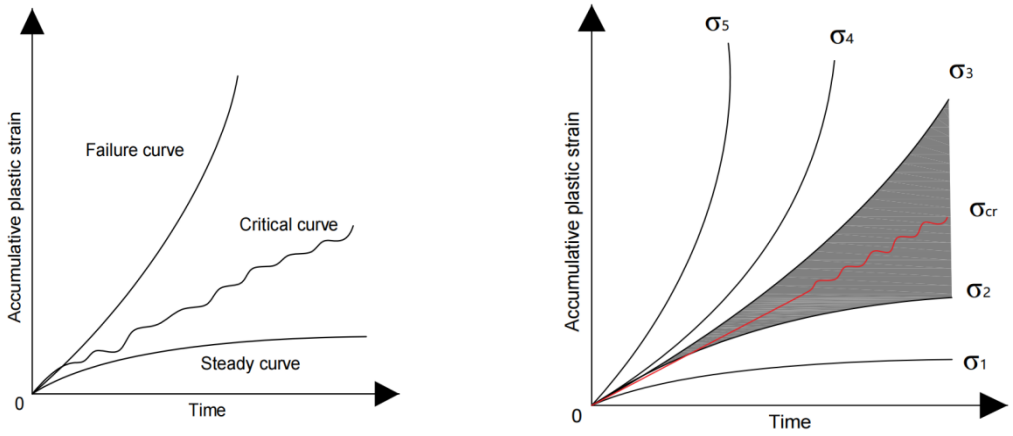

(**a**) (**b**)

Figure 4. (**a**) Representative accumulative strain-time curve; (**b**) Analysis of critical dynamic stress.

2.3. Total Strain of Clay under Long-Term Cyclic Load

Based on the theories above, we ignore any possible contribution of crack or damage to deformation during initial and steady stages. Thus, the corresponding dynamic strain $\varepsilon_d(t)$ of clay can be expressed as

$$\varepsilon_d(t) = \varepsilon_s(t) + \varepsilon_a(t) \tag{8}$$

where $\varepsilon_s(t)$ and $\varepsilon_a(t)$ denote the accumulative plastic strain caused by static stress and alternating stress, respectively. The total dynamic strain-time curve of clay under the long-term cyclic load is plotted in Figure 5.

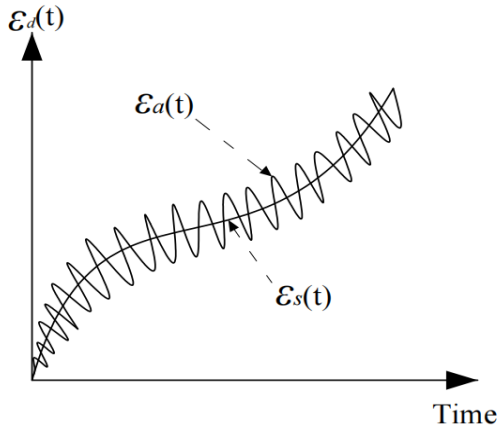

Figure 5. Total dynamic strain-time curve of clay.

3. A Variable-Order Fractional Abel Dashpot

3.1. Mathematical Preliminaries

Definition 1. *Let* $L_1 = L_1(I)$ *be the class of Lebsgue integral functions on the interval* $I = (0, +\infty)$, *and* $f(t) \in L_1$, $\alpha \in (0, +\infty)$, $for\ t > 0$, $Re(\alpha) > 0$, *the Riemann–Liouville integration with the order* α *is defined [42].*

$$D_t^{-\alpha} f(t) = \frac{1}{\Gamma(\alpha)} \int_0^t (t - \tau)^{\alpha - 1} f(\tau) d\tau \tag{9}$$

The fractional derivative is defined as

$$D_t^{\alpha} f(t) = \frac{\mathrm{d}^{\alpha}}{\mathrm{d}t^{\alpha}} \left(\int_0^t (t-\tau)^{\sigma-1} f(\tau) d\tau \right) \tag{10}$$

In the above formula, $D_t^{-\alpha} f(t)$ and $D_t^{\alpha} f(t)$ are the Riemann–Liouville fractional integral operator and derivative operator, respectively; $t > 0, \alpha \geq 0$; n is the smallest positive integer that exceeds α; the order $\sigma = n - \alpha$; and $\Gamma(\alpha)$ is the gamma function $\Gamma(\alpha) = \int_0^{\infty} \mathrm{e}^{-t} t^{\alpha-1} d\tau$.

It can be determined from Equation (9) that the Riemann–Liouville integration with the order α is actually a weighted integral. It is worth noting that, for $\alpha = 1$, the equation is transformed into a common integral, and the weight value is equal to 1; for $\alpha > 1$, the farther the distance between variable t and integral upper limit τ, the larger the weighted value; for $\alpha < 1$, the further the distance between variable t and integral upper limit τ, the smaller the weighted value [43]. The convolution structure fully reflects the temporal dependence of system function development [44]. The Riemann–Liouville fractional calculus is therefore an essential tool for describing the creep behavior of clay.

3.2. The Constant-Order Fractional Abel Dashpot

Clay is characterized by its elasticity, viscoelasticity and plasticity over the course of the entire creep process as shown in Figure 3. The elasticity and plasticity of clay can be described by the hook body and the Newtonian dashpot, respectively, while the viscoelasticity of clay can be described by a constant-order fractional Abel dashpot, as shown in Figure 6.

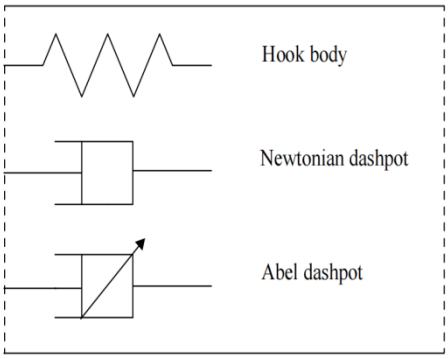

Figure 6. The basic mechanical elements.

The constitutive relationship of the Abel dashpot is given as [45]

$$\sigma(t) = \eta D^{\alpha} \varepsilon(t) \tag{11}$$

where η is the viscosity coefficient, $0 \leq \alpha \leq 1$, and D^{α} indicates fractional differentiation.

When $\alpha = 1$, the Abel dashpot in Equation (11) is a Newtonian dashpot representing an ideal fluid; and the element becomes a spring representing an ideal solid; when $0 < \alpha < 1$, the Abel dashpot can be considered a comprehensive component describing the nonlinear strain processes of the material between the spring and the Newtonian dashpot.

Considering $\sigma(t) = \sigma_0$ (constant stress) in Equation (11), and taking the initial time $t = 0$, by applying the fractional integral to both sides of Equation (11), the equation expression of the Abel dashpot is obtained thus:

$$\varepsilon(t) = \frac{\sigma_0}{\eta} \frac{t^{\alpha}}{\Gamma(1+\alpha)} \tag{12}$$

where σ_0 is the normal level of stress.

By substituting $\sigma_0 = 20$ kPa and $\eta = 40$ kPa $\cdot$ h$^{\alpha}$ into Equation (12), a series of different α creep curves are generated, as shown in Figure 7. Under the condition of equal duration, the greater the order, the greater the creep strain. However, creep strain is not susceptible to the order in the initial stage; with increase in loading duration, the differences among different creep strain curves caused by the order become more distinct.

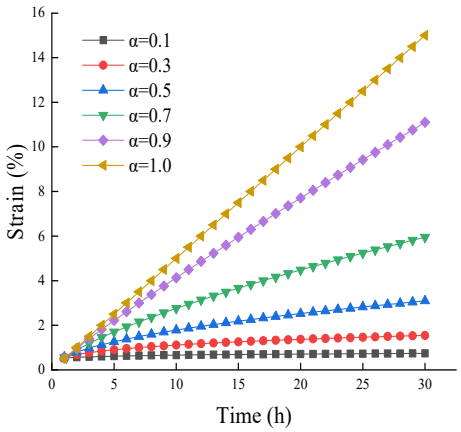

Figure 7. Creep strain under the case of fractional derivative orders characterized by the Abel dashpot.

3.3. The Variable-Order Fractional Abel Dashpot

Because constant-order models are not always suitable to describe the mechanical behavior of the clay, and the mechanical properties of geotechnical materials change with time during the loading process [46], and considering that the mechanical properties of clay can be embodied by the order of fractional calculus, then the order of fractional calculus should also be a variable in the creep process. Assuming the order of fractional calculus to be a function of time in the loading process, i.e., $\alpha = \alpha(t),\ 0 \le \alpha(t) \le 1,\ t > 0$, then the variable-order fractional Abel dashpot is given as follows:

$$\sigma(t) = \eta_{\alpha(t)} D^{\alpha(t)} \varepsilon(t) \tag{13}$$

where $\alpha(t)$ represents the fractional derivative order as a continual function of time.

Let $\alpha(t) = \sigma_0$; by integrating both sides of Equation (13); then, the expression of the variable-order fractional Abel dashpot is given as

$$\varepsilon(t) = \sum_{k=1}^{n} \frac{\sigma_0}{\eta_k} \frac{(t - t_{k-1})^{\alpha_k}}{\Gamma(\alpha_k + 1)} \tag{14}$$

where α_k and η_k represent the order and the viscosity coefficient in different periods, respectively. The variable-order fractional Abel dashpot can now be derived, as in Figure 8.

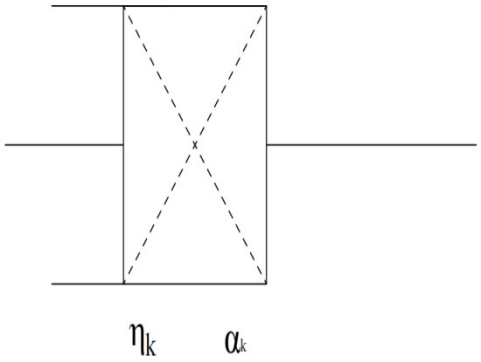

Figure 8. The variable-order fractional Abel dashpot.

4. Establishment of Dynamic Constitutive Model

4.1. Creep Strain of Clay under Long-Term Static Load

According to the previous analysis, we can draw the conclusion that the rheological strain of clay contains instantaneous strain ε_e and viscoelastic strain ε_{ve}, and these can be expressed by the hook body and the variable-order fractional Abel dashpot, respectively. Assuming the stress applied to the sample is equal to σ_0, i.e., $\sigma_0 = (\sigma_{\mathrm{d.max}} + \sigma_{\mathrm{d.min}})/2$, the instantaneous strain can be expressed as

$$\varepsilon_e = \frac{\sigma_0}{E_0} \tag{15}$$

where E_0 is the elastic modulus of the spring in the hook body.

Based on the constitutive model of the variable-order fractional Abel dashpot, the viscoelastic strain expressed as $\varepsilon_{ve.1}(t)$ for the initial creep stage sand $\varepsilon_{ve.2}(t)$ for the steady creep stage can be calculated as follows:

$$\varepsilon_{ve.1}(t) = \frac{\sigma_0}{\eta_1}\frac{(t-0)^{\alpha_1}}{\Gamma(\alpha_1+1)} \tag{16}$$

$$\varepsilon_{ve.2}(t) = \frac{\sigma_0}{\eta_2}\frac{(t-t_1)^{\alpha_2}}{\Gamma(\alpha_2+1)} \tag{17}$$

The viscosity coefficient η_k and the fractional order α_k can be assigned by a mass of values in the creep process, and the relation between η_k and α_k is shown in Table 1. To simplify the final creep constitutive model, two orders were taken out in the initial and steady stages, respectively.

Table 1. Values of fractional order α_k and viscosity coefficient η_k versus time.

Time	Fractional Order α_k	Viscosity Coefficient η_k
$0 < t \le t_1$	α_1	η_1
$t_1 < t \le t_2$	α_2	η_2
⋮	⋮	⋮
$t_{n-1} < t \le t_n$	α_n	η_n

If the stress σ_0 remains unchanged, when the loading duration is in the range of 0 to t_1, the creep constitutive model in initial stage is expressed thus:

$$\varepsilon_s(t) = \varepsilon_e + \varepsilon_{ve.1}(t) = \frac{\sigma_0}{E_0} + \frac{\sigma_0}{\eta_1}\frac{t^{\alpha_1}}{\Gamma(\alpha_1+1)} \quad (0 < t \le t_1) \tag{18}$$

Similarly, in the case of steady stage, we have

$$\varepsilon_s(t) = \varepsilon_{ve.2}(t) = \frac{\sigma_0}{\eta_2}\frac{(t-t_1)^{\alpha_2}}{\Gamma(\alpha_2+1)} \qquad (t_1 < t \le t_2) \tag{19}$$

Whether the clay undergoes the steady stage or the accelerating stage during the loading process mainly depends on the magnitude of σ_0 and on the clay's material properties; when the static load level exceeds the long-term strength σ_s, the clay will experiences accelerating creep; when σ_0 is less than the long-term strength σ_s, the clay will experience decay and steady creep. The entire creep strain of clay can be portrayed by the model based on the variable-order fractional Abel dashpot, as shown in Figure 9.

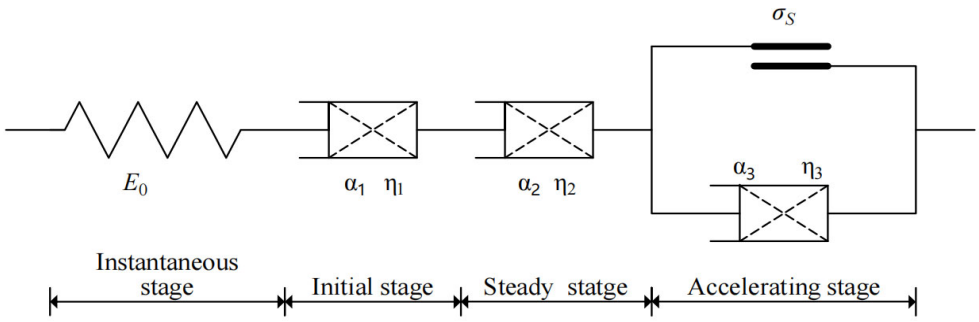

Figure 9. Variable-order fractional creep constitutive model.

For this viscoplastic body, the stress σ_0 of the fractional element is given by

$$\sigma_0 = \begin{cases} 0 & \sigma < \sigma_s \\ \sigma_s & \sigma \ge \sigma_s \end{cases} \tag{20}$$

Although the variable-order Abel dashpot produces a better fit of experimental data in the attenuation and steady stages, when compared with the constant-order Abel dashpot, the method of adjusting these parameters in the variable-order Abel dashpot is not optimal for describing the mechanical properties of clay in the accelerating stage. On the one hand, the order of fractional derivative is related to the state of clay; once the order exceeds 1, the underlying physical meaning is hard to explain. On the other hand, bearing in mind the crack evolution and damage of soil skeleton during the loading process, many researchers [47,48] have introduced damage variables into the viscoplastic body to depict the creep behavior of geotechnical materials. Xu et al. [49] proposed a nonlinear viscoplastic body (NVPB) model to portray creep strain in the accelerating stage for green schist and verified its reliability by experimental data, with the corresponding creep equation given by

$$\varepsilon_c(t) = \frac{H(\sigma_0 - \sigma_s)}{\eta} t^n \tag{21}$$

where σ_0 is the normal stress, n is the rheological index and H can be expressed by

$$H(\sigma_0 - \sigma_s) = \begin{cases} 0 & (\sigma_0 \le \sigma_s) \\ \sigma_0 - \sigma_s & (\sigma_0 > \sigma_s) \end{cases} \tag{22}$$

It will be apparent that the constitutive model has been established by empirical formula without considering structure damages in the soil. Based on the research methods noted above, the damage variable D was introduced into the viscosity coefficient η in this paper, where D assumes damage evolution in the clay rheological process to be a negative exponential function, which can be described as

$$D = 1 - e^{-\beta t} \tag{23}$$

where β is a coefficient related to the properties of the clay, so that the viscoplastic coefficient can be written as

$$\eta = \eta(1 - D) = \eta e^{-\beta t} \tag{24}$$

Therefore, a new viscoplastic body is proposed as shown in Figure 10. Following to the analysis above, a new creep equation for the accelerating stage is given as follows:

$$\varepsilon_c(t) = \frac{H(\sigma_0 - \sigma_s)}{\eta e^{-\beta t}} \tag{25}$$

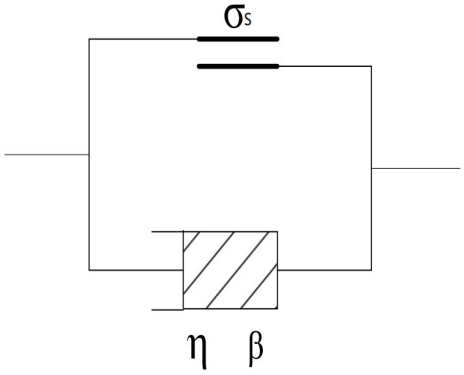

Figure 10. Viscoplastic body.

Bringing together the above, a full creep model for clay under long-term static load can now be obtained, as shown in Figure 11, and the corresponding creep equation can also be determined, so that, when $\sigma_0 \leq \sigma_s$, the creep constitutive equation is expressed as

$$\varepsilon_c(t) = \frac{\sigma_0}{E_0} + \frac{\sigma_0}{\eta_1} \frac{t^{\alpha_1}}{\Gamma(\alpha_1 + 1)} \qquad (0 < t \leq t_1) \tag{26a}$$

$$\varepsilon_c(t) = \frac{\sigma_0}{\eta_2} \frac{(t - t_1)^{\alpha_2}}{\Gamma(\alpha_2 + 1)} \qquad (t_1 < t \leq t_2) \tag{26b}$$

If $\sigma_0 > \sigma_s$

$$\varepsilon_c(t) = \frac{H(\sigma_0 - \sigma_s)}{\eta e^{-\beta t}} \qquad (t > t_2) \tag{26c}$$

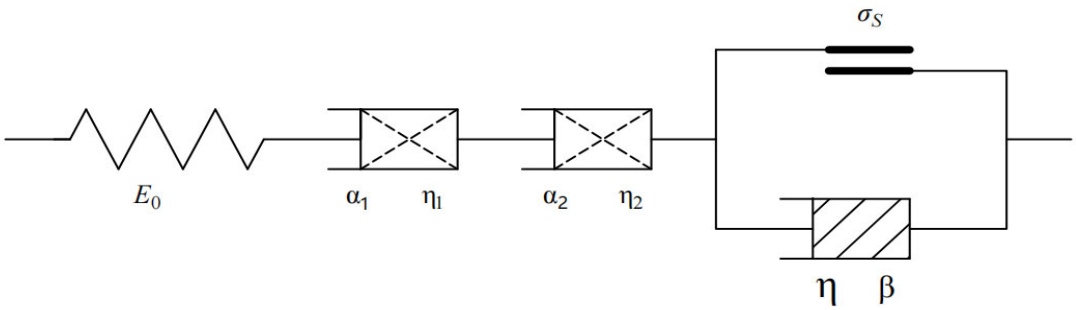

Figure 11. Improved variable-order fractional creep constitutive model.

4.2. The Strain Response of Clay under Long-Term Alternating Load

4.2.1. Dynamic Response Theory of Alternating Strain $\varepsilon_a(t)$

Viscoelastic materials, such as clay, show a viscous effect under subjection to alternating stress, Energy storage and dissipation are continuously accompanied by the process of soil deformation under long-term alternating loading [50]. The phase differences between dynamic strain and dynamic stress for elastic and ideal viscous materials are 0 and $\pi/2$, respectively. Clay is regarded as a kind of viscoelastic material, so that the alternating strain $\varepsilon_a(t)$ lags behind alternating stress $\sigma_a(t)$, assuming that the phase difference between $\varepsilon_a(t)$ and $\sigma_d(t)$ is θ; thus, $0 < \theta < \pi/2$, retardation time is θ/ω, and θ is the complementary angle of energy dissipation angle in viscoelastic mechanics. On the basis of the creep constitutive model portrayed in Figure 11, the alternating stress on clay can be therefore be expressed as

$$\sigma_a(t) = \sigma_1 \sin(wt) = \sigma_1 e^{iwt} \tag{27}$$

where σ_1 is the amplitude of alternating stress, and $\sigma_1 = (\sigma_{\mathrm{d.max}} - \sigma_{\mathrm{d.min}})/2$, while i is the imaginary unit. According to viscoelasticity theory, the strain response can be calculated thus:

$$\varepsilon_a(t) = \varepsilon_1 \sin(wt + \theta) = \varepsilon_1 e^{i(wt+\theta)} = \varepsilon^* e^{iwt} \tag{28}$$

where ε_1 is the amplitude of alternating strain, ε^* is the amplitude of complex strain, and ε_1 and θ are given by

$$\varepsilon_1 = \sigma_1 \sqrt{J_1^2 + J_2^2} \tag{29}$$

$$\theta = \arctan(J_2/J_1) \tag{30}$$

where J_1 and J_2 are represent storage and loss compliance, respectively.

Hook Body

Following the analysis above, the strain response equation of the hook body under alternating stress $\sigma_1 e^{iwt}$ is expressed as

$$\sigma_1 e^{iwt} = E_0 \cdot \varepsilon^* e^{iwt} \tag{31}$$

By rewriting Equation (31) into the form of complex compliance, then

$$J^*(iw) = \frac{\varepsilon^*}{\sigma_1} = \frac{1}{E_0} = J_1 - iJ_2 \tag{32}$$

Where storage compliance $J_1 = 1/E_0$, and loss compliance $J_2 = 0$.

Variable-Order Fractional Abel Dashpot

For the variable-order fractional Abel dashpot, the strain response equation can be derived in accordance with Equation (13) and Fourier transform thus:

$$\sigma_1 e^{iwt} = \eta_{\alpha(t)} (iw)^{\alpha(t)} \varepsilon^* e^{iwt} \tag{33}$$

Equation (33) can be rewritten as

$$J^*(iw) = \frac{\varepsilon^*}{\sigma_1} = \frac{1}{\eta_{\alpha(t)} (iw)^{\alpha(t)}} \tag{34}$$

Due to $(i)^{\alpha(t)} = \cos\left(\frac{\alpha(t)\pi}{2}\right) + i \cdot \sin\left(\frac{\alpha(t)\pi}{2}\right)$, Equation (34) can now be rewritten as

$$\frac{\varepsilon^*}{\sigma_1} = \frac{\cos\left(\frac{\alpha(t)\pi}{2}\right)}{\eta_{\alpha(t)} w^{\alpha(t)}} - i \frac{\sin\left(\frac{\alpha(t)\pi}{2}\right)}{\eta_{\alpha(t)} w^{\alpha(t)}} = J_1 - iJ_2 \tag{35}$$

Accordingly, storage compliance $J_1 = \frac{\cos(\frac{\alpha(t)\pi}{2})}{\eta_{\alpha(t)} w^{\alpha(t)}}$, loss compliance $J_2 = \frac{\sin(\frac{\alpha(t)\pi}{2})}{\eta_{\alpha(t)} w^{\alpha(t)}}$

Viscoplastic Body

For the viscoplastic body, the strain response equation can be derived in accordance with

Equation (25) and Fourier transform, thus:

$$\frac{\varepsilon^*}{\sigma_1} = \frac{e^{\beta t}}{\eta} = J_1 - iJ_2 \tag{36}$$

Consequently, storage compliance $J_1 = \frac{e^{\beta t}}{\eta}$, loss compliance $J_2 = 0$.

4.2.2. The Strain Response of the Creep Constitutive Model

Assuming long-term stress is equal to critical dynamic stress, i.e., $\sigma_s = \sigma_{\mathrm{cr}}$.

(1) when $\sigma_1 \le \sigma_{cr}$,

an expression of strain response based on the creep constitutive model in Figure 11 can be obtained, if the load duration is in the range of 0 to t_1, i.e., $0 < t \le t_1$.

For the initial stage, we find

$$J_{i1} = \frac{1}{E_0} + \frac{\cos(\alpha_1 \pi/2)}{\eta_1 w^{\alpha_1}} \tag{37}$$

$$J_{i2} = \frac{\sin(\alpha_1 \pi/2)}{\eta_1 w^{\alpha_1}} \tag{38}$$

Substituting Equations (37) and (38) into Equations (29) and (30) to reflect the viscous effects of clay under long-term alternating load, the strain response constitutive equation can be expressed as

$$\varepsilon_a(t) = \sigma_1 \sqrt{J_{i1}^2 + J_{i2}^2} \sin\left(wt + \arctan\left(\frac{J_{i2}}{J_{i1}}\right)\right) \tag{39}$$

For the steady stage, we find

$$J_{s1} = \frac{\cos(\alpha_2 \pi/2)}{\eta_2 w^{\alpha_2}} \tag{40}$$

$$J_{s2} = \frac{\sin(\alpha_2 \pi/2)}{\eta_2 w^{\alpha_2}} \tag{41}$$

where $t_1 < t \le t_2$, substituting Equations (40) and (41) into Equations (29) and (30) to reflect the viscous effect, a strain response constitutive equation is given as follows:

$$\varepsilon_a(t) = \sigma_1 \sqrt{J_{s1}^2 + J_{s2}^2} \sin\left(wt + \arctan\left(\frac{J_{s2}}{J_{s1}}\right)\right) \tag{42}$$

(2) When $\sigma_1 > \sigma_{cr}$,

for the accelerating stage, we find

$$J_{a1} = \frac{e^{\beta t}}{\eta} \tag{43}$$

$$J_{a2} = 0 \tag{44}$$

Substituting Equations (43) and (44) into Equations (29) and (30) to reflect the viscous effect, the strain response constitutive equation is given as follows:

$$\varepsilon_a(t) = \sigma_1 \sqrt{J_{a1}^2 + J_{a2}^2} \sin\left(wt + \arctan\left(\frac{J_{a2}}{J_{a1}}\right)\right) \tag{45}$$

where $t > t_2$. As for $0 < t < t_1$ and for $t_1 < t < t_2$, the strain response constitutive equations for the initial and steady stages are identical with Equations (39) and (42), respectively.

4.3. The Dynamic Constitutive Model for Clay

By substituting Equations (26a), (26b), (26c), (39), (42) and (45) into Equation (8), the dynamic constitutive model based on variable-order fractional Abel dashpot, expressing viscoplastic body and strain response is given by

$$\varepsilon_d(t) = \frac{\sigma_0}{E_0} + \frac{\sigma_0}{\eta_1}\frac{(t-0)^{\alpha_1}}{\Gamma(\alpha_1+1)} + \sigma_1\sqrt{J_{i1}^2 + J_{i2}^2}\sin(wt + \arctan(J_{i2}/J_{i1}))\ (0 < t \le t_1) \quad (46)$$

$$\varepsilon_d(t) = \frac{\sigma_0}{\eta_2}\frac{(t-t_1)^{\alpha_2}}{\Gamma(\alpha_2+1)} + \sigma_1\sqrt{J_{s1}^2 + J_{s2}^2}\sin(wt + \arctan(J_{s2}/J_{s1})) \quad (t_1 < t \le t_2) \quad (47)$$

$$\varepsilon_d(t) = \frac{H(\sigma_0 - \sigma_s)}{\eta e^{-\beta t}} + \sigma_1\sqrt{J_{a1}^2 + J_{a2}^2}\sin(wt) \quad (t > t_2) \quad (48)$$

5. Model Validation and Sensitivity Analysis

The applicability and effectiveness of the dynamic constitutive model in Equations (46)–(48) will now be discussed using undrained dynamic triaxial test results for Zhan Jiang clay, and Tian Jin soft clay [51]. In addition, a sensitivity analysis of parameters α_1, α_2, β, η of the dynamic constitutive model will be carried out, using soil parameters taken from the literature [52,53]. The dynamic triaxial test system DYNTTS of the British GDS company was used to perform the test, Sine wave cyclic loading was adopted, and the confining pressure was set to 100 kPa, the vibration frequency was 1 Hz, and the specimen size of the apparatus was 38 mm in diameter and 76 mm in height.

5.1. Model Validation

The efficacy of the dynamic constitutive model is dependent on its ability to adequately fit experimental data; the predictions of the model for the accumulative strain of Zhan Jiang clay and Tian Jin soft clay are shown in Figures 12 and 13, respectively.

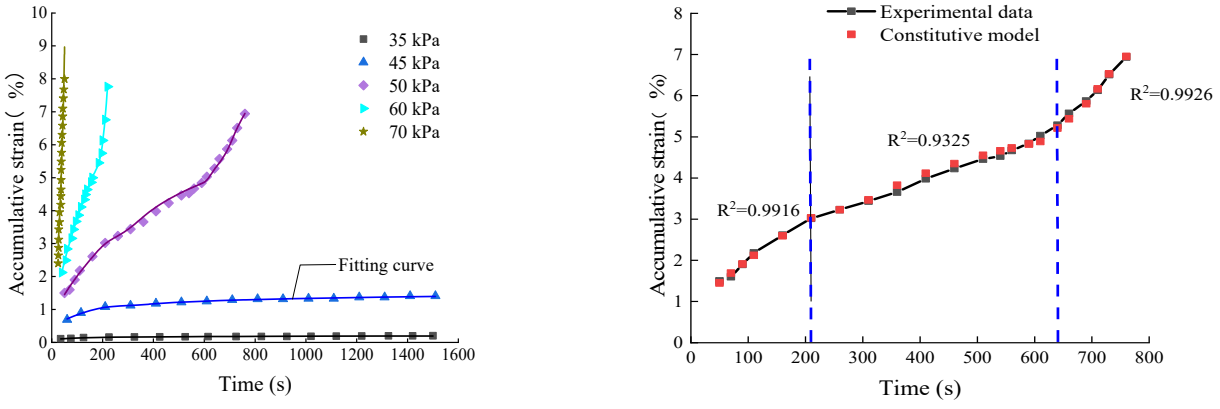

(**a**) (**b**)

Figure 12. (**a**) Predication of dynamic constitutive model in Zhan Jiang clay; (**b**) Comparison between experimental data and fitting results (σ_3 = 100 kPa, σ_1/σ_3 = 0.5).

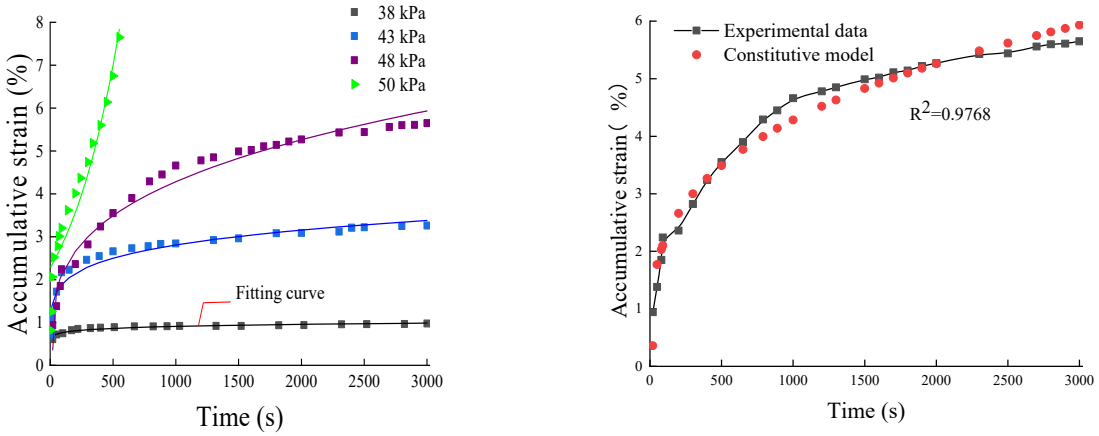

(**a**) (**b**)

Figure 13. (**a**) Predication of dynamic constitutive model in Tian Jin soft clay; (**b**) Comparison between experimental data and fitting results (σ_3 = 100 kPa, σ_1/σ_3 = 0.48).

Since the model agrees well with experimental data for both Zhan Jiang clay and Tian Jin soft clay, given space limitations, the applicability and parameter sensitivity of the model are described based on the test results for Zhan Jiang clay only.

It can be discerned from Figure 12a and Table 2 that the model agrees well with the experimental data, which indicates that the model describes well the steady, critical and failure curves of clay in the dynamic triaxial test. However, it can also be seen that the experimental curves are not always identical with any of the three different types of accumulative strain-time curve. Some experimental curves are normally composed of one to three classical accumulative strain-time curves, so it is potentially inaccurate to say that an accumulative strain-time curve is expressed by only one function expression. In order to obtain an accurate assessment of strain characteristics, our focus of attention must shift from amplitude of stress load on the specimen to determine time points t_1 and t_2 as accurately as we can. The prediction of the model largely depends on t_1 and t_2; for accumulative strain-time curves, the method endows the model with more applicability. In addition, the new constitutive model with damage variables can accurately describe the strain-time characteristics of clay under cyclic load, as shown in Figure 12b, especially in the accelerating stage. Furthermore, as can be understood from Table 2, under the same confining pressure, the orders α and viscosity coefficients η in the initial stage are greater than those in the steady stage, which indicates that the viscous resistance of the soil is reduced. This is because the successive cyclic loading causes the soil to become dense, the soil particles are arranged in a more orderly manner after mutual dislocation and adjustment, and the overall mechanical properties of the soil tend to be ideal when it is solid. Finally, it can be seen from Table 2 that all correlation coefficients have values of more than 0.90, which indicates the accuracy and applicability of the constitutive model, to some extent, at least.

Table 2. Parameters determined via fitting analysis based on the dynamic triaxial test of clay.

σ_d/kPa.	E_0/kPa	α_1	η_1	α_2	η_2	β	η	t_1/s	t_2/s	R^2
	Initial Stage			Steady Stage		Accelerating Stage				
35	1642	0.418	10800					225		0.9497
				0.087	1013			225		0.9006
45	20950	0.354	693					210		0.9926
				0.092	149			210		0.9812
50	184	0.706	1931					210	640	0.9916
				0.254	106			210	640	0.9325

				0.0022	42	210	640	0.9926
60	28050	0.620	519			160		0.9957
				0.0106	72	160		0.9722
70				0.0432	52			0.9391

5.2. Sensitivity Analysis

For completeness, a sensitivity analysis should be performed in order to estimate the influence of the parametric error, Equations (46) to (48) show that the accumulative strain of clay depends on the parameters E_0, α_1, α_2, η_1, η_2, β and η. To more accurately understand the effects of these parameters on the results of each stage and to check the robustness of the constitutive model, a sensitivity analysis was carried out on the main parameters of α_1, α_2, β and η. The results are depicted in Figure 14, which shows the distribution of accumulative strain in different three-dimensional spaces and the respective influences of α_1, α_2, β and η on accumulative strain. Taking the experimental data with 50 kPa amplitude as an example, when one of the parameters of α_1, α_2, β, η is adjusted, other parameters in the model remain the same.

Figure 14a,b show the accumulative strain distributions under the three-dimensional space $t - \alpha_1 - \varepsilon_d$, and the effect of parameter increment $\Delta\alpha_1$ on accumulative strain, respectively. The accumulative strain-time curves under parameter increment $\Delta\alpha_1 = 0.01$ almost coincide in the initial stage. In addition, significant change was no longer observed in dynamic strain once the parameter $\alpha_1 \leq 0.4$ (Figure 14a). Therefore, the influence of parameter α_1 on the accumulative strain is related not only to the $\Delta\alpha_1$, but also to the initial value α_1. On the whole, it was found that there is a certain difference in accumulative strain curves under the parameter increment $\Delta\alpha_1 = 0.01$, but not an obvious difference. Therefore, the parameter α_1 is considered to exhibit low sensitivity in the constitutive model.

Figure 14c,d show accumulative strain distributions under the three-dimensional space $t - \alpha_2 - \varepsilon_d$, and the influence of the parameter increment $\Delta\alpha_2 = 0.01$ on the accumulative strain, respectively. It is worth noting that the accumulative strain increases as the parameter α_2 increases, and the difference in accumulative strain under the parameter increment $\Delta\alpha_2 = 0.01$ is more distinct compared to $\Delta\alpha_1 = 0.01$. The reason for this phenomenon is that the magnitude of the cyclic loading duration becomes larger. Meanwhile, it can be understood from Figure 14c that the accumulative strain calculated by the constitutive model exhibits a lower gradual effect when the order is $0 < \alpha_2 \leq 0.2$. However, when $\alpha_2 > 0.2$, the increase in accumulative strain is more obvious with increasing values of the parameter α_2. Taking into consideration the fitting result above, we therefore concluded that the sensitivity of α_2 to the constitutive model is high.

Figure 14e,f show accumulative strain distributions under the three-dimensional space $t - \beta - \varepsilon_d$, and the influence of the parameter increment $\Delta\beta = 0.2 \times 10^{-3}$ on the accumulative strain, respectively. It can be seen from Figure 14f that the difference in accumulative strain curves under the parameter increment $\Delta\beta = 0.2 \times 10^{-3}$ is obvious. Interestingly, the accumulative strain settled in three-dimensional-space forms an approximate plane with increments in duration and in β, bearing in mind that parameter β is in a negative exponential function, which indicates that the effect of β within a certain magnitude range on the accumulative strain is linear. By comparison with Figure 14d,f, it can be deduced that the sensitivity of β to the constitutive model is significantly powerful.

Figure 14g,h show the accumulative strain distributions under the three-dimensional space $t - \eta - \varepsilon_d$, and the effect of the parameter increment $\eta = 10$ on the accumulative strain, respectively. As η increases, the starting point of the accumulative strain moves down. In addition, it is clear from Figure 14g that the variation of accumulative strain is especially striking when the parameter η is $0 < \eta < 100$. Therefore, the sensitivity of η to the constitutive model is also significantly powerful, especially in the range of 0 to 100.

On the whole, the sensitivity of α_1, α_2, β and η to the constitutive model exhibits a growing trend with increments of loading duration, but it is hard to determine merely by a figure whether the sensitivity of these parameters to the constitutive model is powerful or weak in a certain range; once they exceed a certain range, they may exhibit a trend in opposition to the model.

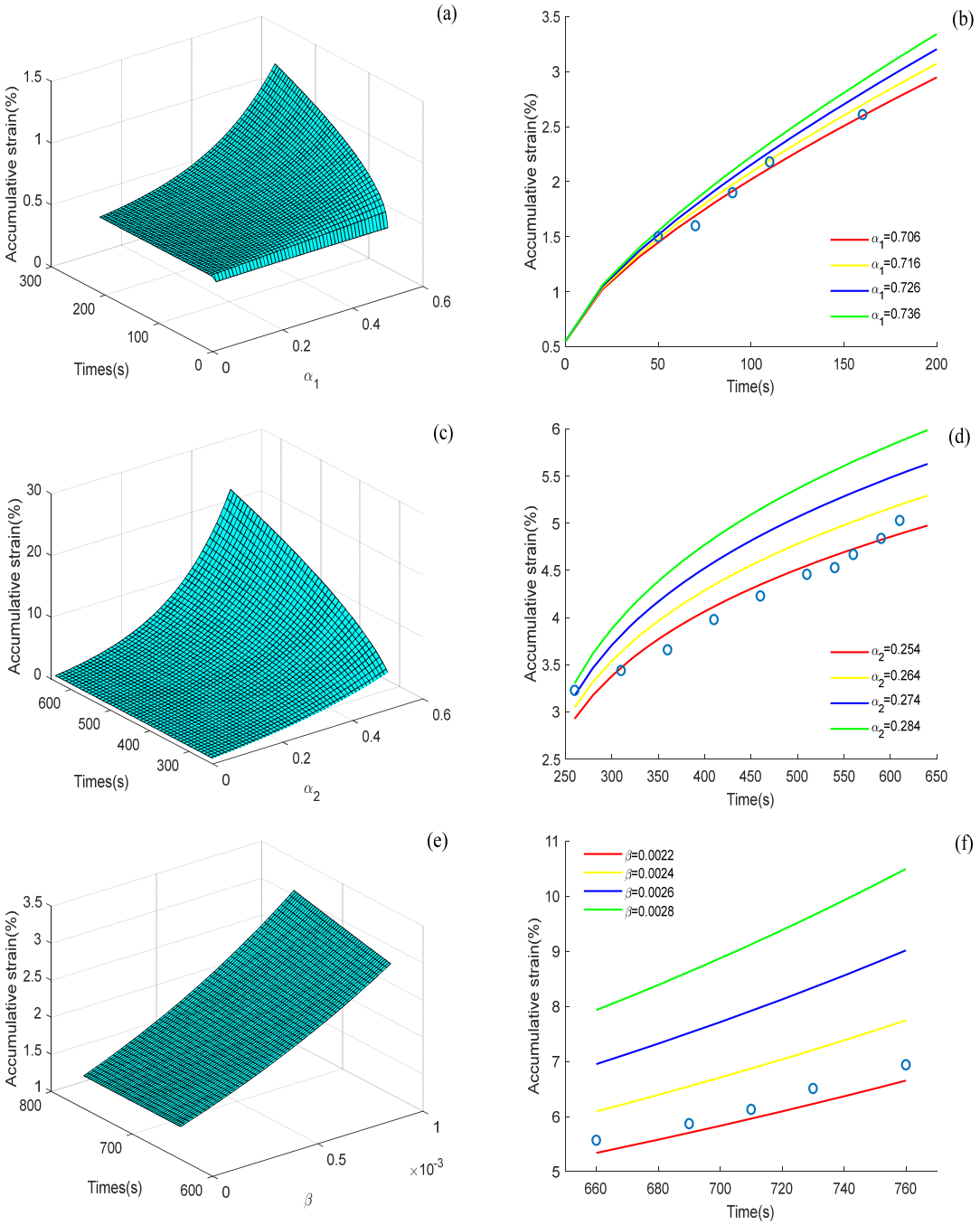

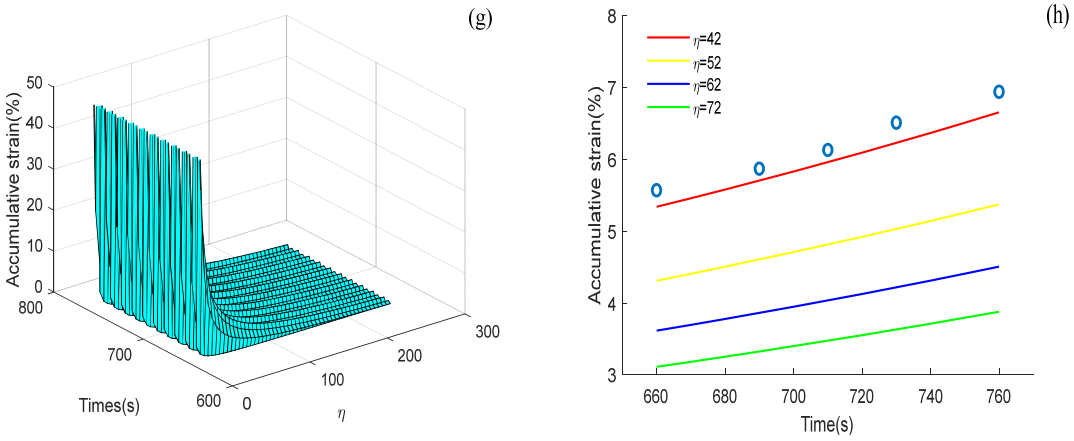

Figure 14. Sensitivity analysis of parameters α_1, α_2, β and η of the constitutive model.

5.3. Comparison of Models

To date, many dynamic constitutive models for soil have been proposed by scholars, and these models have been adapted for various situations. These include the exponential model initially proposed by Monismith, a hyperbolic model, an improved exponential model which considers the effect of stress levels, and an improved hyperbolic model [14,51,54,55]. On the whole, the ability of such models to fit the accumulative strain curve has become better and better. Equations for the models described above are given by Equations (49) to (52).

Exponential model [14]:

$$\varepsilon_d(t) = aN^b \tag{49}$$

Hyperbolic mode [54]:

$$\varepsilon_d(t) = \frac{N}{a + bN} \tag{50}$$

Improved exponential model [55]:

$$\varepsilon_d(t) = a\left(\frac{\sigma_d}{\sigma_s}\right)^m N^b \tag{51}$$

Improved hyperbolic model [51]:

$$\varepsilon_d(t) = d(\delta^N - 1) + \frac{bN^m}{1 + cN^m} \tag{52}$$

where N represents circulation times, and $t = NT$, where T is the period of cyclic load, and a, b, c, m are all fitting parameters. δ expresses the state of soil, d is the form factor of accumulative strain, and the fitting results of different models are plotted in Figure 15.

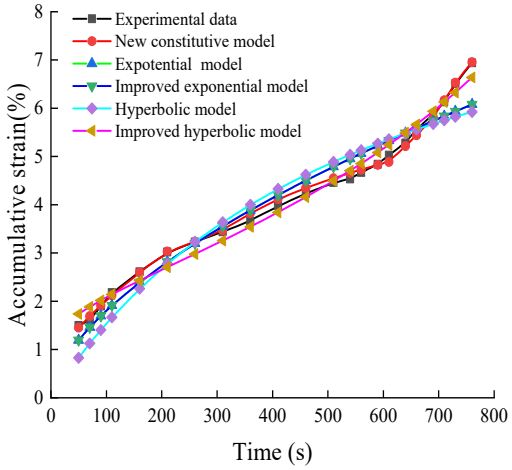

Figure 15. Comparison of fitting effects of different models.

It can be seen from Figure 15 that the prediction abilities of the dynamic constitutive model presented in this paper and the improved hyperbolic model are significantly higher than those of the exponential model, improved exponential model and hyperbolic model. By comparing the fitting results of the new dynamic constitutive model and the improved hyperbolic model for the accelerating stage, we find that the new dynamic constitutive model is almost completely consistent with the experimental data, which indicates that the viscoplastic body can well describe the deformation characteristics of clay in the accelerating stage.

6. Discussion

Although a new constitutive model of clay under long-term dynamic stress has been constructed, and described in this paper, some questions still need to be discussed and many further studies need to be carried out:

The new constitutive model with damage variables for clay was built based on fractional calculus theory, and the univariate constitutive model equations were derived and verified by citing undrained dynamic triaxial test data. But what are the three-dimensional constitutive model equations? The model needs to be extended and verified further.

In addition, the loading duration used in our study was a relatively short time, and the efficacy of the new constitutive model remains to be verified by more experimental data in future.

It should also be noted that the new constitutive model is obtained by successive loading, and it does well characterize the accumulative strain of clay under long-term dynamic stress. However, soil deformation occurs intermittently in most cases, such as the deformation of filling materials used for embankments. It is therefore essential that the effects of intermittent load on accumulative strain be considered in future studies.

Finally, in practice, soil deformation is affected by confining pressure, deviatoric stress, stress history and vibration frequency amongst other factors. It is therefore necessary to introduce new variables for better describing the deformation of clay in different situations.

7. Conclusions

Based on half-sine wave characteristics, the dynamic stress of clay can be separated into static and alternating stress, and the corresponding accumulative strain consists of creep dominated by static and strain responses ruled by dynamic stress. According to the

theories of fractional calculus, rheology, soil dynamics and viscoelastic mechanics, a constitutive model of clay under long-term loading can be established to predict the accumulative strain.

By analyzing the applicability and effectiveness of the constitutive model, whose ability to predict the accumulative strain of clay under long-term dynamic stress has been verified, by comparison with different models, and by sensitivity analysis of parameters, we can state our main conclusions as follows:

[I] A new dynamic constitutive model suitable for describing the accumulative strain of clay is proposed. Instantaneous strain, viscoelastic strain and viscoplastic strain within total accumulative strain are described by means of hook body, variable-order Abel dashpot and viscoplastic body, respectively.

[II] The new constitutive model proposed in this paper was applied to fit the undrained dynamic triaxial data under the action of the amplitude of dynamic stress. According to the fitting results, all correlation coefficients exceed 0.9, which indicates to some extent that the ability of the new constitutive model can characterize the accumulative strain of clay under long-term cyclic loading.

[III] By analyzing the accumulative strain of clay under the actions of parameter increments, the sensitivity effect of parameters α_1, α_2, β and η was revealed, and the interaction mechanisms among parameters, loading duration and accumulative strain was clarified. The influence of parameters α_1, α_2, β and η upon accumulative strain was clearly demonstrated.

[IV] In comparison with other constitutive models, the new constitutive model presented in this paper exhibits a significantly higher predictive performance, especially for the accelerating stage, which illustrates that the viscoplastic body method described in this paper can well characterize the deformation characteristics of clay in the accelerating stage.

Author Contributions: B.-L.Z.: writing—review and editing; K.-S.C.: validation; X.H.: validation; K.Z.: validation. All authors have read and agreed to the published version of the manuscript.

Funding: This work was funded by the Science and Technology Support Program of Guizhou Province (Qian Ke He Support [2020] No. 4Y038).

Data Availability Statement: Some or all data, models, or code that support the findings of this study are available from the corresponding author upon reasonable request.

Conflicts of Interest: Author Bo-Lang Zhang declares that he has no conflict of interest. Author Kai-Sheng Chen declares that he has no conflict of interest. Author Xing Hu declares that he has no conflict of interest. Author Kun Zhang declares that he has no conflict of interest.

References

1. Jin, Q.; Zheng, Y.-J.; Cui, X.-Z.; Cui, S.-Q.; Qi, H.; Zhang, X.-N.; Wang, S. Evaluation of dynamic characteristics of silt in Yellow River Flood Field after freeze-thaw cycles. *J. Cent. South Univ.* **2020**, *27*, 2113–2122. https://doi.org/10.1007/s11771-020-4434-7.
2. Shen, S.-L.; Wu, H.-N.; Cui, Y.-J.; Yin, Z.-Y. Long-term settlement behaviour of metro tunnels in the soft deposits of Shanghai. *Tunn. Undergr. Space Technol.* **2014**, *40*, 309–323. https://doi.org/10.1016/j.tust.2013.10.013.
3. Jongpradist, P.; Youwai, S.; Jaturapitakkul, C. Effective Void Ratio for Assessing the Mechanical Properties of Cement-Clay Admixtures at High Water Content. *J. Geotech. Geoenviron. Eng.* **2011**, *137*, 621–627. https://doi.org/10.1061/(asce)gt.1943-5606.0000462.
4. Fortunato, E.; Paixão, A.; Morais, P.; Santos, C.; Morais, J.; Cruz, J.; Cruz, N. Subgrade reinforcement of old railway tracks using short soil–binder columns—Laboratory studies and field tests. *Transp. Geotech.* **2021**, *29*, 100577. https://doi.org/10.1016/j.trgeo.2021.100577.
5. Fattah, M.Y.; Mahmood, M.R.; Aswad, M.F. Stress distribution from railway track over geogrid reinforced ballast underlain by clay. *Earthq. Eng. Eng. Vib.* **2019**, *18*, 77–93. https://doi.org/10.1007/s11803-019-0491-z.
6. Zhu, S.; Chen, R.-P.; Yin, Z.-Y. Elastoplastic modeling of cyclic behavior of natural structured clay with large number of cycles. *Transp. Geotech.* **2021**, *26*, 100448. https://doi.org/10.1016/j.trgeo.2020.100448.
7. Truong, M.H.; Indraratna, B.; Nguyen, T.T.; Carter, J.; Rujikiatkamjorn, C. Analysis of undrained cyclic response of saturated soils. *Comput. Geotech.* **2021**, *134*, 104095. https://doi.org/10.1016/j.compgeo.2021.104095.

8. Ni, J.; Indraratna, B.; Geng, X.-Y.; Carter, J.P.; Chen, Y.-L. Model of Soft Soils under Cyclic Loading. *Int. J. Geomech.* **2015**, *15*, 04014067. https://doi.org/10.1061/(asce)gm.1943-5622.0000411.
9. Corti, R.; Diambra, A.; Wood, D.M.; Escribano, D.E.; Nash, D.F.T. Memory Surface Hardening Model for Granular Soils under Repeated Loading Conditions. *J. Eng. Mech.* **2016**, *142*, 04016102. https://doi.org/10.1061/(asce)em.1943-7889.0001174.
10. Zhao, H.Y.; Indraratna, B.; Ngo, T. Numerical simulation of the effect of moving loads on saturated subgrade soil. *Comput. Geotech.* **2021**, *131*, 103930. https://doi.org/10.1016/j.compgeo.2020.103930.
11. Shih, J.-Y.; Grossoni, I.; Bezin, Y. Settlement analysis using a generic ballasted track simulation package. *Transp. Geotech.* **2019**, *20*, 100249. https://doi.org/10.1016/j.trgeo.2019.100249.
12. Zuada Coelho, B.; Dijkstra, J.; Karstunen, M. Viscoplastic cyclic degradation model for soft natural soils. *Comput. Geotech.* **2021**, *135*, 104176. https://doi.org/10.1016/j.compgeo.2021.104176.
13. Deng, Q.-L.; Ren, X.-W. An energy method for deformation behavior of soft clay under cyclic loads based on dynamic response analysis. *Soil Dyn. Earthq. Eng.* **2017**, *94*, 75–82. https://doi.org/10.1016/j.soildyn.2016.12.012.
14. Monismith, C.L.; Ogawa, N.; Freeme, C.R. Permanent deformation characteristics of subgrade soil due to repeated loading. *Transp. Res. Rec. J. Transp. Res. Board* **1975**, *537*, 1–17.
15. Chawla, S.; Shahu, J.T.; Kumar, S. Analysis of cyclic deformation and post-cyclic strength of reinforced railway tracks on soft subgrade. *Transp. Geotech.* **2021**, *28*, 100535. https://doi.org/10.1016/j.trgeo.2021.100535.
16. He, L.-L.; Wang, Y.-Z.; Li, S.-Z.; Wang, Z.-Y. Practical method and application study for predicting cyclic accumulative deformations of the saturated soft clay. *J. Mt. Sci.* **2017**, *14*, 2348–2358. https://doi.org/10.1007/s11629-016-3972-9.
17. Chen, C.; Zhou, Z.; Zhang, X.; Xu, G. Behavior of amorphous peaty soil under long-term cyclic loading. *Int. J. Geomech.* **2018**, *18*, 04018115. https://doi.org/10.1061/(asce)gm.1943-5622.0001254.
18. Salour, F.; Rahman, M.S.; Erlingsson, S. Characterizing Permanent Deformation of Silty Sand Subgrades by Using a Model Based on Multistage Repeated-Load Triaxial Testing. *Transp. Res. Rec. J. Transp. Res. Board* **2016**, *2578*, 47–57. https://doi.org/10.3141/2578-06.
19. Xu, X.; Zhang, W.; Fan, C.; Lai, Y.; Wu, J. Effect of freeze–thaw cycles on the accumulative deformation of frozen clay under cyclic loading conditions: Experimental evidence and theoretical model. *Road Mater. Pavement Des.* **2019**, *22*, 925–941. https://doi.org/10.1080/14680629.2019.1696221.
20. Hu, Z.; Wang, R.; Ren, X.; Wei, X.; Wang, Q. Permanent deformation behavior of compacted loess under long-term traffic loading. *J. Mater. Civ. Eng.* **2019**, *31*, 04019157. https://doi.org/10.1061/(asce)mt.1943-5533.0002815.
21. Sun, Q.; Cai, Y.; Chu, J.; Dong, Q.; Wang, J. Effect of variable confining pressure on cyclic behaviour of granular soil under triaxial tests. *Can. Geotech. J.* **2017**, *54*, 768–777. https://doi.org/10.1139/cgj-2016-0439.
22. Sas, W.; Gluchowski, A.; Gabrys, K.; Sobol, E.; Szymanski, A. Resilient Modulus Characterization of Compacted Cohesive Subgrade Soil. *Appl. Sci.* **2017**, *7*, 370. https://doi.org/10.3390/app7040370.
23. Nie, R.; Li, Y.; Leng, W.; Mei, H.; Dong, J.; Chen, X. Deformation characteristics of fine-grained soil under cyclic loading with intermittence. *Acta Geotech.* **2020**, *15*, 3041–3054. https://doi.org/10.1007/s11440-020-00955-3.
24. Thevakumar, K.; Indraratna, B.; Ferreira, F.B.; Carter, J.; Rujikiatkamjorn, C. The influence of cyclic loading on the response of soft subgrade soil in relation to heavy haul railways. *Transp. Geotech.* **2021**, *29*, 100571. https://doi.org/10.1016/j.trgeo.2021.100571.
25. Kabwe, E.; Karakus, M.; Chanda, E.K. Creep constitutive model considering the overstress theory with an associative viscoplastic flow rule. *Comput. Geotech.* **2020**, *124*, 103629. https://doi.org/10.1016/j.compgeo.2020.103629.
26. Song, Z.; Song, W.; Cheng, Y.; Yang, T.; Wang, T.; Wang, K. Investigation on Strain Characteristics and Fatigue Constitutive Model of Limestone under Osmotic Pressure and Cyclic Disturbance Coupling. *Ksce J. Civ. Eng.* **2022**, *26*, 1740–1753. https://doi.org/10.1007/s12205-022-1416-3.
27. Zhu, Z.-Y.; Luo, F.; Zhang, Y.-Z.; Zhang, D.-J.; He, J.-L. A creep model for frozen sand of Qinghai-Tibet based on Nishihara model. *Cold Reg. Sci. Technol.* **2019**, *167*, 102843. https://doi.org/10.1016/j.coldregions.2019.102843.
28. Lyu, C.; Liu, J.; Zhao, C.; Ren, Y.; Liang, C. Creep-damage constitutive model based on fractional derivatives and its application in salt cavern gas storage. *J. Energy Storage* **2021**, *44*, 103403. https://doi.org/10.1016/j.est.2021.103403.
29. Zhang, J.; Yao, B.; Ao, Y.; Jin, C.; Sun, C. Analysis and numerical calculation of a coupled creep and strain-softening model for soft rock tunnels. *PLoS ONE* **2021**, *16*, e0256243. https://doi.org/10.1371/journal.pone.0256243.
30. Zhao, Y.; Wang, Y.; Wang, W.; Wan, W.; Tang, J. Modeling of non-linear rheological behavior of hard rock using triaxial rheological experiment. *Int. J. Rock Mech. Min. Sci.* **2017**, *93*, 66–75. https://doi.org/10.1016/j.ijrmms.2017.01.004.
31. Xu, M.; Jin, D.; Song, E.; Shen, D. A rheological model to simulate the shear creep behavior of rockfills considering the influence of stress states. *Acta Geotech.* **2018**, *13*, 1313–1327. https://doi.org/10.1007/s11440-018-0716-8.
32. Zhang, S.; Liu, W. The 3D Nonstationary Creep Constitutive Model of Sandstone Based on Fractional Order. *Math. Probl. Eng.* **2019**, *2019*, 1–12. https://doi.org/10.1155/2019/6031842.
33. Yan, B.; Guo, Q.; Ren, F.; Cai, M. Modified Nishihara model and experimental verification of deep rock mass under the water-rock interaction. *Int. J. Rock Mech. Min. Sci.* **2020**, *128*, 104250. https://doi.org/10.1016/j.ijrmms.2020.104250.
34. Pu, S.; Zhu, Z.; Song, L.; Song, W.; Peng, Y. Fractional-order visco-elastoplastic constitutive model for rock under cyclic loading. *Arab. J. Geosci.* **2020**, *13*, 1–11. https://doi.org/10.1007/s12517-020-05288-9.
35. Madaschi, A.; Gajo, A. A one-dimensional viscoelastic and viscoplastic constitutive approach to modeling the delayed behavior of clay and organic soils. *Acta Geotech.* **2017**, *12*, 827–847. https://doi.org/10.1007/s11440-016-0518-9.

36. Kamoun, J.; Bouassida, M. Creep behavior of unsaturated cohesive soils subjected to various stress levels. *Arab. J. Geosci.* **2018**, *11*, 77. https://doi.org/10.1007/s12517-018-3399-4.
37. Li, J.; Yang, Y. Creep behavior of unsaturated reticulate red clay under matric suction. *KSCE J. Civ. Eng.* **2017**, *22*, 582–587. https://doi.org/10.1007/s12205-017-0092-1.
38. Liu, J.; Jing, H.; Meng, B.; Wang, L.; Yang, J.; You, Y.; Zhang, S. Fractional-order creep model for soft clay under true triaxial stress conditions. *Arab. J. Geosci.* **2020**, *13*, 1–13. https://doi.org/10.1007/s12517-020-05842-5.
39. Oliveira, P.J.V.; Santos, S.L.; Correia, A.A.S.; Lemos, L.J.L. Numerical prediction of the creep behaviour of an embankment built on soft soils subjected to preloading. *Comput. Geotech.* **2019**, *114*, 103140. https://doi.org/10.1016/j.compgeo.2019.103140.
40. Zhang, Q.; Leng, W.; Zhai, B.; Xu, F.; Dong, J.; Yang, Q. Evaluation of Critical Dynamic Stress and Accumulative Plastic Strain of an Unbound Granular Material Based on Cyclic Triaxial Tests. *Materials* **2021**, *14*, 5722. https://doi.org/10.3390/ma14195722.
41. Mu, R.; Huang, Z.H.; Pu, S.Y.; Hua, Y.Z.; Cheng, X. Accumulated deformation characteristics of undisturbed red clay under cyclic loading and dynamic constitutive relationship. *Rock Soil Mech.* **2020**, 1–10. https://doi.org/10.16285/j.rsm.2020.0719.
42. Kilbas, A.; Srivastava, H.M.; Trujillo, J.J. *Theory and Applications of Fractional Differential Equations*; Elsevier: Amsterdam, The Netherlands, 2006.
43. Wu, Q.; Huang, J.H. *Fractional Calculus*; Tsinghua University Press: Beijing, China, 2016.
44. Wu, F.; Zhang, H.; Zou, Q.; Li, C.; Chen, J.; Gao, R. Viscoelastic-plastic damage creep model for salt rock based on fractional derivative theory. *Mech. Mater.* **2020**, *150*, 103600. https://doi.org/10.1016/j.mechmat.2020.103600.
45. Scott Blair, G.W. The role of psychophysics in rheology. *J. Colloid Sci.* **1947**, *2*, 21–32. https://doi.org/10.1016/0095-8522(47)90007-X.
46. Wu, F.; Liu, J.; Zou, Q.L.; Li, C.B.; Chen, J.; Gao, R.B. A triaxial creep model for salt rocks based on variable-order fractional derivative. *Mech. Time-Depend. Mater.* **2020**, *25*, 101–118. https://doi.org/10.1007/s11043-020-09470-0.
47. Chen, B.-R.; Zhao, X.-J.; Feng, X.-T.; Zhao, H.-B.; Wang, S.-Y. Time-dependent damage constitutive model for the marble in the Jinping II hydropower station in China. *Bull. Eng. Geol. Environ.* **2013**, *73*, 499–515. https://doi.org/10.1007/s10064-013-0542-z.
48. Liu, J.; Wu, F.; Zou, Q.; Chen, J.; Ren, S.; Zhang, C. A variable-order fractional derivative creep constitutive model of salt rock based on the damage effect. *Geomech. Geophys. Geo-Energy Geo-Resour.* **2021**, *7*, 1–16. https://doi.org/10.1007/s40948-021-00241-w.
49. Xu, W.Y.; Yang, S.Q.; Xie, S.Y.; Shao, J.F.; Wang, Y.F. Investigation on triaxial rheological mechanical properties of greenschist specimen (II): Model analysis. *Rock Soil Mech.* **2005**, *26*, 693–698. https://doi.org/10.16285/j.rsm.2005.05.004.
50. Pu, S.Y.; Rao, J.Y.; Yang, K.Q.; Huang, Z.H.; Li, Y.H.; Chen, Z.N.; Li, Q.; Liu, H.Q. Deformation characteristics of soil under cyclic loading. *Rock Soil Mech.* **2017**, *38*, 3261–3270. https://doi.org/10.16285/j.rsm.2017.11.023.
51. Zang, M.; Kong, L.W.; Cao, Y. An improved model for cumulative deformations of clay subjected to cyclic loading. *Rock Soil Mech.* **2017**, *38*, 435–442. https://doi.org/10.16285/j.rsm.2017.02.017.
52. Cao, Y. Study on Load Waveform Effect of Dynamic Characteristics and on Damage Properties of Structure Soft Soil. Ph.D.Thesis, State Key Laboratory of Geomechanics and Engineering, Wuhan Institute of Geomechanics, Chinese Academy of Sciences, Wuhan, Hubei, 2013.
53. Zang, M.; Kong, L.W.; Guo, A.G. Effects of static deviatoric stress on dynamic characteristics of Zhanjiang structured clay. *Rock Soil Mech.* **2017**, *38*, 33–40. https://doi.org/10.16285/j.rsm.2017.01.005.
54. Zhu, Y.H.; Liu, G.B.; Xie, Q.F.; Zheng, R.Y. Cumulative plastic strain model of soft clay considering temperature effect and its verification. *China Earthq. Eng. J.* **2019**, *41*, 901–907, 961. https://doi.org/10.3969/j.issn.1000-0844.2019.04.901.
55. Li, Y.F.; Nie, R.S.; Li, Y.J.; Leng, W.M.; Ruan, B. Cumulative plastic deformation of subgrade fine-grained soil under intermittent cyclic loading and its prediction model. *Rock Soil Mech.* **2021**, *42*, 1065–1077. https://doi.org/10.16285/j.rsm.2020.1210.